2007 Fall Meeting of the Western States Section of the Combustion Institute
Sandia National Laboratories, Livermore, CA
October 16 & 17, 2007.

Theoretical Rate Coefficients for the Reaction of Methyl Radical and Hydroperoxyl Radical and for Methylhydroperoxide Decomposition

Ahren W. Jasper,[1] Stephen J. Klippenstein,[2] and Lawrence B. Harding[2]

[1] *Combustion Research Facility, Sandia National Laboratories, PO Box 969, Livermore, CA 94551-0969, USA*

[2] *Chemistry Division, Argonne National Laboratory, Argonne, IL 60439, USA*

The kinetics of the $CH_3 + HO_2$ bimolecular reaction and the thermal decomposition of CH_3OOH are studied theoretically. Direct variable reaction coordinate transition state theory (VRC-TST) is used to compute the high pressure limit rate coefficient for the $CH_3 + HO_2$ reaction and to characterize the transition state region of the barrierless $CH_3O + OH$ product channel. The $CH_2O + H_2O$ product channel is treated using variational transition state theory and the harmonic oscillator and rigid rotor approximations. Pressure dependence and product branching are modeled using master equation simulations. The predicted rate coefficients for the major products channels of the bimolecular reaction, $CH_3O + OH$ and $CH_4 + O_2$, are found to be in excellent agreement with values obtained in two recent modeling studies.

1. Introduction

In combustion systems at moderate temperatures and high pressures, stabilization of $H + O_2$ to form hydroperoxyl radicals is favored over explosive chain branching, and CH_3 and HO_2 are the dominant species in the radical pool. In some systems, their reaction competes with methyl recombination as the major sink for CH_3, and the relative significance of these pathways for CH_3 consumption has important consequences, as the hydroperoxyl reaction produces reactive OH and O_2, whereas the recombination reaction is chain terminating. For example, in one modeling study of CH_4/O_2 at high pressures,[1] the $CH_3 + HO_2$ reaction was found to be an important source of OH during ignition, and the authors identified this reaction as one requiring further study.

The bimolecular reaction of methyl radical and hydroxyl radical may proceed via an energized complex

$$\begin{aligned} CH_3 + HO_2 \rightarrow CH_2OOH^* (+M) &\rightarrow CH_3O + OH && (1a)\\ &\rightarrow CH_2O + H_2O && (1b)\\ &\rightarrow CH_3OOH && (1c) \end{aligned}$$

or directly via hydrogen abstraction

$$\begin{aligned} CH_3 + HO_2 &\rightarrow CH_4 + {}^3O_2 && (1d)\\ &\rightarrow CH_4 + {}^1O_2\,. && (1e) \end{aligned}$$

Direct measurements of the rate coefficients for reaction 1 have not been made. Based on one set of indirect measurements,[2] Baulch et al.[3] recommended $k_{1a} = 3 \times 10^{-11}$ cm^3 molecule^{-1} s^{-1} for 600–1200 K with an uncertainty of an order of magnitude.

Scire et al.[4,5] perturbed the well characterized lean moist CO oxidation system with methane and used flow reactor experiments and modeling studies to extract rate coefficients for the two major product channels of reaction 1 (1a and 1d). Under their conditions and in the absence of CH_4, CO is primarily consumed by OH. At low pressures (~1 atm) and when small amounts of CH_4 were added to the system, CO oxidation was found to be suppressed, as CH_4 consumed OH much faster than CO. At high pressures, however, the addition of CH_4 was found to increase the rate of CO oxidation. The authors identified the $CH_3 + HO_2$ reaction as an important process at high pressures, and the resulting formation of $CH_3O + OH$ and $CH_4 + O_2$, both of which are chain propagating, explained the increased combustion of CO. The rate coefficients they obtained ($k_{1a} = 2.46 \times 10^{-11}$ and $k_{1d} = 5.25 \times 10^{-12}$ cm^3 molecule^{-1} s^{-1} at 1000 K) agree with the previous estimate[3] and have considerably reduced uncertainties.

We also consider the thermal decomposition of methylhydroperoxide

$$\begin{aligned} CH_3OOH &\rightarrow CH_3O + OH && (2a)\\ &\rightarrow CH_2O + H_2O && (2b)\\ &\rightarrow CH_3OOH && (2c) \end{aligned}$$

which has been previously studied experimentally[6] over a limited temperature range (600–700 K). This value was adopted in a recent review.[3]

Theoretical predictions of the kinetics of reactions 1 and 2 are complicated by the presence of the barrierless channels $CH_3 + HO_2$ and $CH_3O + OH$. Zhu and Lin[7] previously characterized the CH_3OOH system using high level electronic structure theory and variational transition state theory. The rate coefficients they obtained for reactions 1 and 2 are largely in good agreement with the limited experimental data. The rate coefficient for 1a at 1000 K, however, was predicted to be ~3 times larger than the value obtained in the modeling studies of Scire et al.,[4,5] and this difference is close to but greater than the uncertainty ascribed to the measured value. In the theoretical study, the flux through the transition state for the barrierless channels was evaluated using the harmonic oscillator and rigid rotor approximations, and, while this approximation is appropriate in many cases, the accuracy of the harmonic oscillator approximation for describing the density of states of barrierless reactions is questionable.

Variable reaction coordinate transition state theory[8,9,10] (VRC-TST) has been developed to accurately treat barrierless reactions, and its direct implementation, in which the interaction potential of the reacting fragments is evaluated on-the-fly using multireference electronic structure calculations, allows for the efficient computation of quantitative rate coefficients. In recent studies[11,12] of systems with as many as eight carbon atoms, the VRC-TST method was shown to be computationally practical and to predict rate coefficients with estimated errors of less than 25% for a series of hydrocarbon radical-radical association reactions. The ab initio VRC-TST method was also recently used to describe the kinetics of the $CH_3 + OH$ association reaction with similar accuracy.[13]

The goal of the present study is to use direct VRC-TST calculations, high level electronic structure theory, variational transition state theory, and master equation simulations to characterize the CH_3OOH system and obtain rate coefficients for reactions 1 and 2. The methods used here were recently validated for the experimentally well characterized CH_3OH system,[13] where good agreement was obtained between theory and a wide variety of experiment results.

In Sec. 2, details of the kinetics methods and electronic structure methods used are discussed. Results are presented in Sec. 3. Section 4 is a summary.

2. Theory

2.A. Potential Energy Surfaces

For the VRC-TST barrierless rate calculations for the $CH_3 + HO_2$ and $CH_3O + OH$ reactions, the interaction potential energy surface was obtained by fixing the structures of the reacting fragments at their isolated B3LYP/6-311++G(d,p)[14,15] equilibrium geometries. The remaining degrees of freedom, describing the relative orientation and separation of the fragments, were treated as fully coupled to one another and anharmonic, and the interaction potential was computed on-the-fly using multireference perturbation theory[16] (CASPT2).

The active spaces for the CASPT2 calculations were chosen to be the minimum required to correctly describe the separated fragments: two electrons in two orbitals for the $CH_3 + HO_2$ reaction, and six electrons in four orbitals for the $CH_3O + OH$ reaction. To avoid root flipping problems when evaluating the $CH_3O + OH$ interaction energy, orbitals were optimized to minimize the average energy of the four lowest-energy states, which correlate asymptotically with the doubly degenerate $^2\Pi$ state of OH and the doubly degenerate ground state of C_{3V} CH_3O. The neglect of Jahn-Teller distortion in CH_3O simplifies the rate calculations and is not a significant additional source of error, as discussed elsewhere[13] for the $CH_3O + H$ reaction. A level shift[17] of 0.3 E_h (1 E_h = 627.5 kcal/mol) was applied in all of the CASPT2 calculations. The cc-pVDZ, aug-cc-pVDZ, and aug-cc-pVTZ Dunning basis sets[18,19] were used, and basis set convergence will be discussed in Sec. 3.

For the $CH_3O + OH$ reaction, the spin-orbit splitting associated with the $^2\Pi$ state of the OH fragment was included as follows. Uncoupled energies for the two lowest-energy doublet states and the two lowest-energy quartet states were computed using state-averaged CASPT2 calculations and the active space and basis sets discussed above. Spin-orbit perturbations to the uncoupled energies were computed using state averaged CASSCF/6-311++G(d,p) wave functions and the Breit-Pauli operator,[20] and spin-orbit split energies were obtained by diagonalizing the resulting energy matrix.

Stationary point and channel energies were computed using B3LYP/6-311++G(d,p) geometries and QCISD(T)[21,22] energies extrapolated to the complete basis set (CBS) limit using the formula[23]

$$E_{\text{cc-pV}x\text{Z}} = E_{\text{CBS}} + \frac{B}{(n_x + 1)^4} \quad (3)$$

where $n_T = 3$ and $n_Q = 4$ for the cc-pVTZ and cc-pVQZ basis sets,[18] respectively. The Q_1 diagnostic[24] was used to estimate the importance of multireference effects and thereby the reliability of the QCISD(T) calculations. For most of the systems, the Q_1 diagnostic was less than ~0.02, suggesting that the QCISD(T) method is appropriate for these systems. For HO_2 and for the saddle point for H abstraction on the singlet surface (1e), the Q_1 diagnostic was 0.04.

Reaction enthalpies at 0 K were obtained using harmonic B3LYP/6-311++G(d,p) zero point energies and are summarized in Table 1, where they are compared with experimental values from the online NIST database.[25] The QCISD(T)/CBS//B3LYP/6-311++G(d,p) energetics are in good agreement with the experimental results, with a root-mean-square errors of only 1.0 kcal/mol. Zhu and Lin[7] previously characterized this system using G2M theory,[26] and the results are also shown in Table 1 and Fig. 1.

Table 1: Reaction enthalpies and stationary point energies at 0 K (kcal/mol)

Reaction	Present[a]	Zhu and Lin[b]	Experimental[c]
$CH_3 + HO_2 \rightarrow$			
$CH_3O + OH$	–24.47	–24.8	–24.9 ± 1.2
$CH_4 + {}^1O_2$	–25.56	–29.4	
$CH_4 + {}^3O_2$	–54.8[d]	–58.2	–54.7 ± 0.7
CH_3OOH	–67.11	–70.5	–67.3[e]
$CH_2O + H_2O$	–122.88	–126.1	–121.0 ± 0.7
$[CH_3OOH \Leftrightarrow CH_2O + H_2O]^{\ddagger}$ (SP1)	–19.33	–24.1	
$[CH_3 + HO_2 \Leftrightarrow CH_4 + {}^3O_2]^{\ddagger}$ (SP2)	–1.9[d]	–0.7	
$[CH_3 + HO_2 \Leftrightarrow CH_4 + {}^1O_2]^{\ddagger}$ (SP3)	20.2	4.1	
${}^3[H_3C\cdots HO_2]^{\ddagger}$ (vdW)	–2.5[d]	–1.9	
RMS deviation from experiment	1.0	3.5	

[a]QCISD(T)/CBS//B3LYP/6-311++G(d,p)
[b]Previous theoretical results[7] obtained using G2M theory
[c]Obtained from the NIST online database[25]
[d]From Ref. 27
[e]Adjusted from 298 K using B3LYP/6-311++G(d,p) frequencies and rotational constants

The saddle point for H abstraction on the triplet surface (1d) could not be located at the B3LYP/6-311++G(d,p) level of theory. The reverse process was previously characterized[27] in detail using CCSD(T)/aug-cc-pVDZ geometries and frequencies and CCSD(T)/aug-cc-pVTZ energetics. Good agreement between theory and experiment was obtained in that study over a wide temperature range. In the present study, we therefore simply adopt the previous theoretical values, transformed via the equilibrium constant obtained using the geometries, frequencies and energetics calculated in Ref. 27.

The kinetics of the minor product channel 1e is not considered in the present work.

The Gaussian program package[28] was used to perform the density functional theory calculations and geometry optimizations, and the Molpro program package[29] was used to perform the QCISD(T), CASPT2, and spin-orbit calculations.

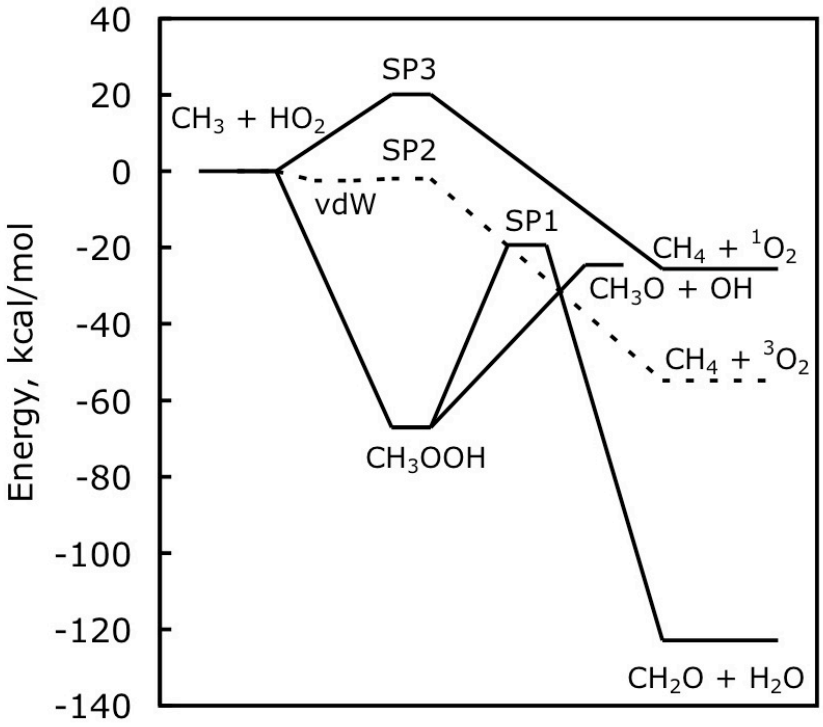

Figure 1: Calculated channel energies and stationary point energies at 0 K

2.B. Rate Calculations

Rate coefficients for the barrierless reactions were obtained using the VRC-TST method,[8,9,10] as implemented in the computer code VaReCoF.[30] In the VRC-TST method, nuclear motions are classified as either conserved or transitional modes,[31] where conserved modes correspond to the internal motions of the isolated fragments and transitional modes correspond to rigid fragment rotations and translations at large fragment separations and participate in bond formation, relative rotations, and overall rotation at intermediate distances. Conserved modes are assumed to evolve adiabatically along the reaction path, and they are treated as separable from one another and from the transitional modes, i.e., fragment relaxation at finite fragment separations is neglected. The transitional modes, which typically have low frequencies and are highly anharmonic, are treated classically and as fully anharmonic and coupled to one another. The flux for the transitional modes is obtained via Monte Carlo sampling, and the flux for the conserved modes is obtained using the harmonic oscillator approximation and frequencies set to those of the isolated fragments. This prescription allows for an efficient evaluation of the flux through transition state dividing surfaces appropriate for barrierless reactions, while retaining the most important mode-mode couplings and anharmonicities.

The geometry dependence of the optimal dividing surface for barrierless reactions may vary significantly as a function of total energy E, total angular momentum J, and temperature. In the

present work, several types of dividing surfaces were considered, and the optimal dividing surface for each E,J pair was determined variationally. Thermal rate coefficients were then obtained by averaging over the microcanonically optimized fluxes with the appropriate Boltzmann weights.

For both the $CH_3 + HO_2$ and $CH_3O + OH$ reactions, center of mass (CoM) dividing surfaces were used, where these dividing surfaces are defined in terms of a fixed CoM separation of the reacting fragments. CoM dividing surfaces are expected to be appropriate at low temperatures, where centrifugal barriers at large fragment separations are the dynamical bottlenecks for association.

At higher temperatures, the dominant centrifugal barriers occur at shorter fragment separations where chemical bonding begins to take place, and variable reaction coordinate (VRC) dividing surfaces are generally more appropriate. When multiple sites are available for bonding, multifaceted (MF) VRC dividing surfaces, described in detail elsewhere,[32] are required. VRC and MF dividing surfaces are obtained by defining one or more pivot point locations for each fragment around which the fragment is allowed to rotate rigidly. The pivot points need not be located at an atomic center or at the center of mass of the fragment. For radical-radical reactions, pivot points are typically displaced from the atom participating in bond formation along the singly occupied orbital. A minimum separation for each pair of pivot points located on different fragments is then defined, and the overall dividing surface is obtained by considering geometries which do not violate any of the minimum separation criteria and which have at least one pivot point separation equal to its minimum allowed value. The resulting dividing surface is continuous and may therefore be variationally optimized with respect to the fragment separation and the location of the pivot points. For the $CH_3 + HO_2$ reaction, MF dividing surfaces with pivot points displaced from the carbon atom out of the plane of the CH_3 fragment and displaced from the terminal O atom and out of the plane of the HO_2 fragment were considered.

The VRC-TST rate calculations were corrected for dynamical recrossing using the transmission coefficient obtained in a previous trajectory study[12] of hydrocarbon radical-radical association reactions. This value was found to be 0.85 and independent of temperature.

Rovibronic coupling (i.e., the angular momentum coupling of the electronic and rotational degrees of freedom) has a significant effect on the total partition function of the reactant OH, especially at low temperatures. For transition state species at sufficiently large fragment separations, the effect of rovibronic coupling may be expected to be similar to that of OH, whereas, for shorter fragment separations, the effect of rovibronic coupling is less clear. This coupling is neglected in the VRC-TST calculations, and, if we assume that the effect of rovibronic coupling at the transition state is similar to that for the reactant OH, it is appropriate to neglect rovibronic coupling when computing the partition function for OH. We chose to treat the electronic partition function for OH classically and as uncoupled to rotation in a previous study of the $CH_3 + OH$ reaction, and good agreement was obtained with experimental results for that system.

The kinetics of the $CH_2O + H_2O$ channel was characterized using the rigid rotor and harmonic oscillator approximations and variational transition state theory. This approach is appropriate for

reactions with large barriers and "tight" transition states, as is the case for the $CH_2O + H_2O$ reaction. The B3LYP/6-311++G(d,p) method was used to compute the minimum energy path and frequencies, and the QCISD(T)/CBS method was used to determine the energetics.

3. Results and Discussion

The best present theoretical prediction of the rate coefficient for each of the reactions discussed in this section was fit to a modified Arrhenius expression, and the results are summarized in Table 2.

Table 1: Capture rate coefficients fit to $A(T/298\ \mathrm{K})^n\exp(-E/T)$ for T = 300–2500 K

Reaction	A (cm^3 $molecule^{-1}$ s^{-1})	n	E (K)
$CH_3 + HO_2$[a]	6.905×10^{-12}	0.3081	–391.9
$CH_3 + HO_2$[b]	6.426×10^{-14}	2.228	–1521.
$CH_3O + OH$	4.600×10^{-11}	0.02337	–81.24
$CH_2O + H_2O$[c]	1.356×10^{-15}	3.322	50490

[a]Total rate coefficient for the indirect reaction (1a–1c)
[b]Direct abstraction on the triplet surface (1d)
[c]1500–2500 K

3.A. High Pressure Limit Rate Coefficients

$CH_3 + HO_2$. VRC-TST capture rate coefficients for the $CH_3 + HO_2$ reaction are shown in Fig. 2 for the CASPT2 method and the cc-pVDZ and aug-cc-pVDZ basis sets. The cc-pVDZ rate coefficient is 10–25% lower than the aug-cc-pVDZ result.

Basis set sensitivity was further tested using the basis set correction potential (BSCP) scheme, as discussed elsewhere.[11] Briefly, a one-dimensional BSCP was previously developed[33] as a function of the forming C–O bond distance and was defined as the energy difference along the minimum energy path for association of a reference reaction ($CH_3 + OH$) computed using a high level basis set (aug-cc-pVTZ) and a low level basis set (cc-pVDZ or aug-cc-pVDZ). The BSCP was then used to correct the energies obtained in a full dimensional VRC-TST calculation with the potential evaluated at the low level of theory. For hydrocarbon reactions, this scheme was previously shown[11] to give aug-cc-pVTZ-quality rate coefficients at the computational cost of a cc-pVDZ calculation. Furthermore, BSCPs obtained using the $CH_3 + CH_3$ and $CH_3 + H$ reference reactions were shown[11,12] to work well for substituted radical–radical hydrocarbon reactions. For the $CH_3 + OH$, reaction, however, the BSCP scheme was found[13,33] to significantly degrade the accuracy of the calculation if the cc-pVDZ basis set was used as the low level of theory. If the aug-cc-pVDZ basis set was used as the low level of theory, the results were found to be similar to those obtained using the uncorrected aug-cc-pVDZ and aug-cc-pVTZ basis sets and to agree with experiment within 30%. For the present system, as shown in Fig. 2, we again find that using the BSCP scheme to correct the cc-pVDZ energies results in a significant increase in the predicted rate coefficient, while the corrected and uncorrected aug-cc-pVDZ results are in close agreement with one another. We may conclude from these results that the predicted rate coefficient is well converged at the aug-cc-pVDZ level and that the cc-pVDZ surface is qualitatively incorrect.

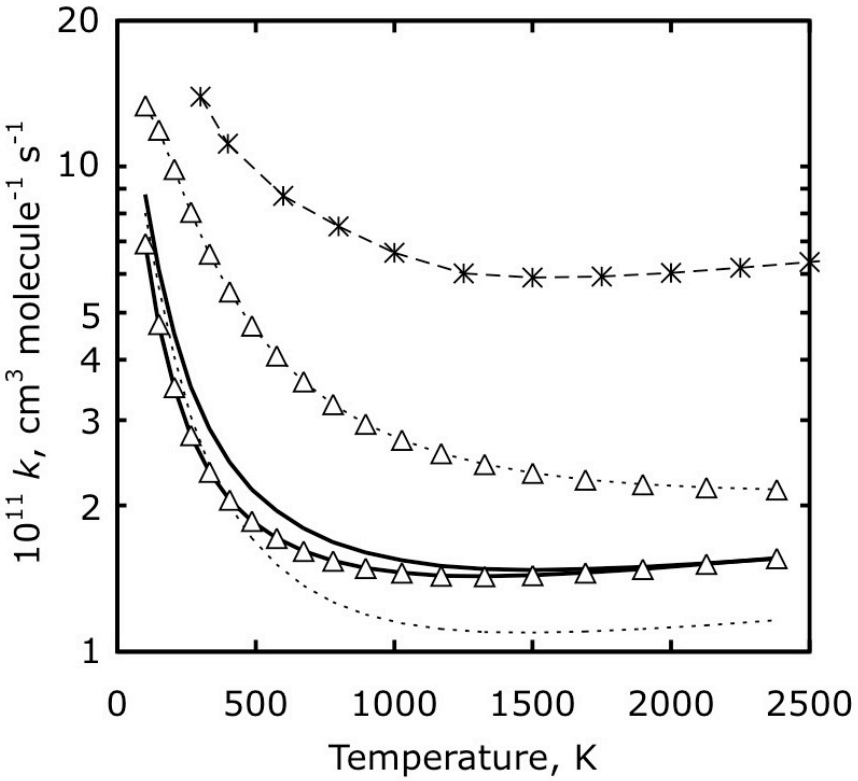

Figure 2. VRC-TST capture rate coefficient for the CH_3 + HO_2 indirect reaction (1a–1c) computed using the the cc-pVDZ (dashed) and aug-cc-pVDZ (solid) basis sets with (triangles) and without (no symbols) using a one-dimensional basis set correction potential. Also shown is the previous theoretical prediction of Zhu and Lin (*).

Next we consider the theoretical description of the transition state dividing surface in the VRC-TST calculations. The inclusion of dividing surfaces with MF pivot points on both fragments lowers the predicted rate coefficient by 10% at room temperature (as compared with the rate coefficient obtained by considering CoM dividing surface exclusively), and the effect is negligible at temperatures above 1000 K. Dividing surfaces with MF pivot points on the CH_3 fragment and a single pivot point on the HO_2 fragment lower the predicted rate coefficient by 12% at high temperatures and are negligible at temperatures below 1000 K.

CH_3O + OH. The CH_3O + OH barrierless association reaction was computed using the VRC-TST method and the CASPT2 electronic structure method, as discussed above. The VRC-TST prediction is weakly dependent on basis set, differing by less than 5% for the cc-pVDZ and aug-cc-pVDZ basis sets. The inclusion of the geometry dependent spin–orbit correction has a small effect (less than 4%). Tsang and Hampson previously estimated this reaction to have a rate coefficient of 3 x 10^{-11} cm^3 molecule^{-1} s^{-1}, which is close to the present prediction of 5–6 x 10^{-11} cm^3 molecule^{-1} s^{-1} for 300–2500 K. We do not consider the abstraction processes, as we are interested in characterizing the $CH_3OOH \Leftrightarrow CH_3O$ + OH process.

CH_2O + H_2O. The $CH_2O + H_2O \rightarrow CH_3OOH$* process has a forward barrier height of 102 kcal/mol and is endothermic by 56 kcal/mol. The reverse of this process may be expected to compete with the barrierless O–O bond scission, as the transition state is close in only 5 kcal/mol

higher than to the channel energy of CH_3O + OH. The "tight" transition state for this process, however, has a much less dense manifold of states than the "loose" CH_3O + OH transition state, and the latter is expected to be the dominant decay pathway for the CH_3OOH* complex.

3.B. CH_3 + HO_2 Bimolecular Collisions

The temperature and pressure dependence of the product branching in reactions 1a–1c was modeled using master equation simulations. The parameters and methods used are the same as those that were recently used to describe the kinetics of the CH_3OH system, and are discussed in detail elsewhere.[13] The exclusive product (<99%) of the indirect reaction mechanism (1a–1c) is CH_3O + OH for pressures up to at least 100 atm for temperatures from 300–2500 K. At very high pressures (much greater than 100 atm), stabilization of the complex becomes important. The CH_2O + H_2O product channel makes up no more than 1% of the total reaction at any of the conditions considered here.

Figure 3 shows the temperature dependence of the rate coefficients for the two major product channels (1a and 1d). Also shown are the experimental values of Scire et al.[4,5] at 1000 K and the previous theoretical predictions of Zhu and Lin.[7] Both sets of theoretical values agree well with the measured rate for k_{1d} at 1000 K. The present value for k_{1a} is within the estimated experimental uncertainty, whereas the previous theoretical prediction of Zhu and Lin is somewhat higher. Although there are several differences between the theoretical treatment of the Zhu and Lin and the one employed here, it is likely that the major difference in the predicted rate coefficient is the treatment of the barrierless transition state, and the present use the VRC-TST method is expected to be generally more accurate.

Curran and Pitz[34] have obtained rate coefficients for reactions 1a and 1d based on detailed modeling studies, and their values are also shown in Fig. 3. Agreement with the present predicted values is excellent.

3.C. CH_3OOH Dissociation

The competitive dissociation of the CH_3OOH complex was modeled using master equations simulations, as described elsewhere.[13] The complex has two torsional modes, which were treated as hindered rotors. The H_3C–OOH torsion has a period of 60^o and a torsional barrier of 2.75 kcal/mol. The CH_3O–OH torsion has a period of 180^o and a torsional barrier of 5.31 kcal/mol.

The exclusive product channel for 300–2500 K and 0.1–100 atm is CH_3O + OH. The predicted rate coefficients at 1 atm is in excellent agreement with Zhu and Lin,[7] and are within a factor of two of the experimental values of Lightfoot et al.[6] from 600–700 K.

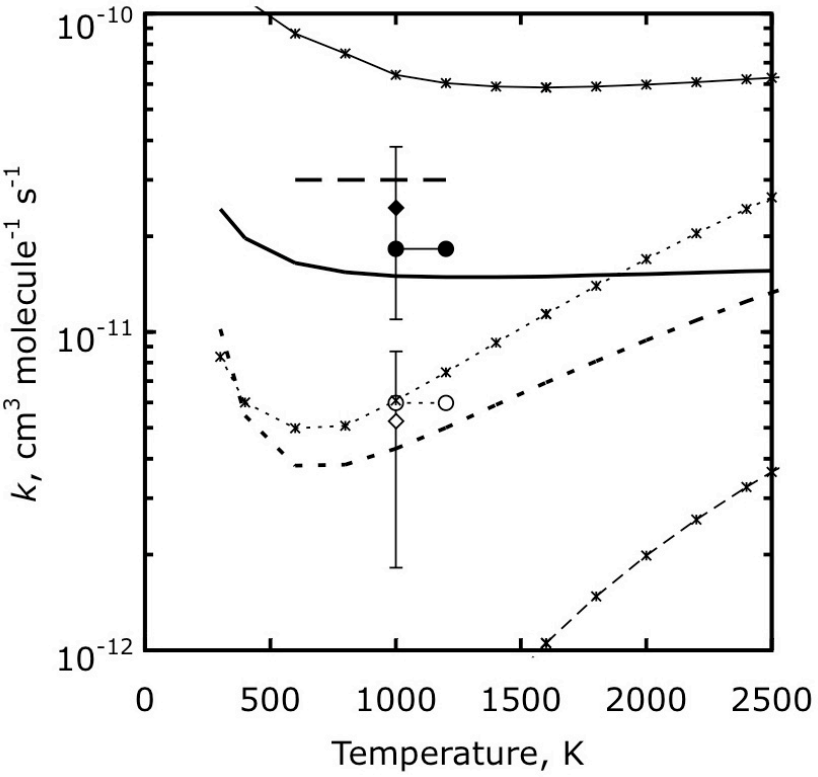

Figure 3. Present predicted rate coefficients for the $CH_3 + HO_2 \rightarrow CH_3O + OH$ (thick solid) and $CH_4 + O_2$ (thick dotted) reactions. The previous theoretical results of Zhu and Lin are also shown (thin lines with * symbols), including the rate coefficient for the $CH_4 + {}^1O_2$ channel (dashed). The measured values from Refs. 4 and 5 are shown as diamonds, and those from Ref. 34 are shown as circles, where open and closed symbols denote the $CH_4 + O_2$ and $CH_3O + OH$ products, respectively. The recommended value of Baulch et al.[3] (with the product unspecified) is shown as a thick dashed line.

4. Conclusions

A theoretical study of the kinetics of the $CH_3 + HO_2$ bimolecular reaction and the decomposition of CH_3OOH has been performed for a wide range of temperatures and pressures, including those relevant to combustion. Rate coefficients were determined using a combination of *ab initio* calculations, variational transition state theory, and master equation simulations, and comparisons were made with available experimental and previous theoretical results. Agreement between the present values for the rate coefficients for the bimolecular reaction and those obtained in two sets of recent modeling studies is excellent.

Acknowledgments

This work was performed under the auspices of the Office of Basic Energy Sciences, Division of Chemical Sciences, Geosciences, and Biosciences, U.S. Department of Energy, in part under contract number DE-AC02-06CH11357.

References

[1] Petersen, E. L.; Davindson, D. F.; Hanson, R. K. *Combust. Flame* **1999**, *117*, 272.
[2] Colket, M. B.; Naegeli, D. W.; Glassman, I. *Symp. (Int.) Combustion*, 1977, *16*, 1023.
[3] Baulch, D. L.; Bowman, C. T.; Cobos, C. J.; Cox, R. A.; Just, Th.; Kerr, J. A.; Pilling, M. J.; Stocker, D.; Troe, J.; Tsang, W.; Walker, R. W.; Warnatz, *J. Phys. Chem. Ref. Data* **2005**, *34*, 757.
[4] Scire, Jr, J. J.; Yetter, R. A.; Dryer, F. L. *Int. J. Chem. Kinetics* **2001**, *33*, 75.
[5] Scire, Jr, J. J.; Dryer, F. L.; Yetter, R. A. *Int. J. Chem. Kinetics* **2001**, *33*, 784.
[6] Lightfoot, P. D.; Roussel, P.; Caralp, F.; Lesclaux, R. *J. Chem. Soc. Faraday Trans.* **1991**, *87*, 3213.
[7] Zhu, R.; Lin, M. C. *J. Phys. Chem. A* **2001**, *105*, 6243.
[8] Klippenstein, S. J. *J. Chem. Phys.* **1992**, *96*, 367.
[9] Klippenstein, S. J. *J. Phys. Chem.* **1994**, *98*, 11459.
[10] Georgievskii, Y.; Klippenstein, S. J. *J. Chem. Phys.* **2003**, *118*, 5442.
[11] Harding, L. B.; Georgievskii, Y.; Klippenstein, S. J. *J. Phys. Chem. A* **2005**, *109*, 4646.
[12] Klippenstein, S. J.; Georgievskii, Y.; Harding, L. B. *Phys. Chem. Chem. Phys.* **2006**, *10*, 1133.
[13] Jasper, A. W.; Klippenstein, S. J.; Harding, L. B.; Ruscic, B. *J. Phys. Chem. A* **2007**, *111*, 3929.
[14] Becke, A. D. *J. Chem. Phys.* **1993**, *98*, 5648. Lee, C.; Yang, W.; Parr, R. G. *Phys. Rev. B* **1998**, *37*, 785.
[15] Krishnan, R.; Binkley, J. S.; Seeger, R.; Pople, J. A., *J. Chem. Phys.* **1980**, *72*, 650. Clark, T.; Chadrasekhar, J.; Schleyer, P. v. R. *J. Comp. Chem.* **1993**, *4*, 294.
[16] Andersson, K.; Malmqvist, P.-A.; Roos, B. O. *J. Chem. Phys.* **1992**, *96*, 1218. Werner, H.-J. *Mol. Phys.* **1996**, *89*, 645. Celani, P.; Werner, H.-J. *J. Chem. Phys.* **2000**, *112*, 5546.
[17] Roos, B. O.; Andersson, K. *Chem. Phys. Lett.* **1995**, *245*, 215. Celani, P.; Werner, H.-J. *J. Chem. Phys.* **2003**, *119*, 5044.
[18] Dunning, Jr., T. H. *J. Chem. Phys.* **1989**, *90*, 1007.
[19] Kendall, R. A.; Dunning, Jr., T. H.; Harrison, R. J. *J. Chem. Phys.* **1992**, *96*, 6796.
[20] Berning, A.; Schweizer, M.; Werner, H.-J.; Knowles, P. J.; Palmier, P. *Mol. Phys.* **2000**, *98*, 1823.
[21] Pople, J. A.; Head-Gordon, M.; Raghavachari, K. *J. Chem. Phys.* **1987**, *87*, 5968. Raghavachari, K.; Trucks, G. W.; Pople, J. A.; Head-Gordon, M. *Chem. Phys. Lett.* **1989**, *157*, 479.
[22] The ROHF-RQCISD(T) algorithm is used for the open shell QCISD(T) calculations. See Knowles, P. J.; Hampel, C.; Werner, H.-J. *J. Chem. Phys.* **1993**, *99*, 5219, *ibid.*, **2000**, *112*, 3106(E).
[23] Martin, J. M. L.; Uzan, O. *Chem. Phys. Lett.* **1998**, *282*, 16.
[24] Lee, T. J.; Rendell, A. P.; Taylor, P. R. *J. Phys. Chem.* **1990**, *94*, 5463.
[25] NIST Computational Chemistry Comparison and Benchmark Database, NIST Standard Reference Database Number 101 Release 12, Aug 2005, Editor: Russell D. Johnson III, http://srdata.nist.gov/cccbdb.
[26] Mebel, A. M.; Morokuma, K.; Lin, M. C. *J. Chem. Phys.* **1995**, *103*, 7414.
[27] Srinivasan, N. K.; Michael, J. V.; Harding, L. B.; Klippenstein, S. J. *Combust. Flame* **2007**, *149*, 104.

[28] Gaussian 98, Revision A.7, Frisch, M. J.; Trucks, G. W.; Schlegel, H. B.; Scuseria, G. E.; Robb, M. A.; Cheeseman, J. R.; Montgomery, Jr., J. A.; Vreven, T.; Kudin, K. N.; Burant, J. C.; Millam, J. M.; Iyengar, S. S.; Tomasi, J.; Barone, V.; Mennucci, B.; Cossi, M.; Scalmani, G.; Rega, N.; Petersson, G. A.; Nakatsuji, H.; Hada, M.; Ehara, M.; Toyota, K.; Fukuda, R.; Hasegawa, J.; Ishida, M.; Nakajima, T.; Honda, Y.; Kitao, O.; Nakai, H.; Klene, M.; Li, X.; Knox, J. E.; Hratchian, H. P.; Cross, J. B.; Bakken, V.; Adamo, C.; Jaramillo, J.; Gomperts, R.; Stratmann, R. E.; Yazyev, O.; Austin, A. J.; Cammi, R.; Pomelli, C.; Ochterski, J. W.; Ayala, P. Y.; Morokuma, K.; Voth, G. A.; Salvador, P.; Dannenberg, J. J.; Zakrzewski, V. G.; Dapprich, S.; Daniels, A. D.; Strain, M. C.; Farkas, O.; Malick, D. K.; Rabuck, A. D.; Raghavachari, K.; Foresman, J. B.; Ortiz, J. V.; Cui, Q.; Baboul, A. G.; Clifford, S.; Cioslowski, J.; Stefanov, B. B.; Liu, G.; Liashenko, A.; Piskorz, P.; Komaromi, I.; Martin, R. L.; Fox, D. J.; Keith, T.; Al-Laham, M. A.; Peng, C. Y.; Nanayakkara, A.; Challacombe, M.; Gill, P. M. W.; Johnson, B.; Chen, W.; Wong, M. W.; Gonzalez, C.; Pople, J. A.; Gaussian, Inc., Wallingford CT, 2004.

[29] MOLPRO, Version 2006.1, Werner, H.-J.; Knowles, P. J.; Lindh, R.; Manby, F. R.; Schütz, M.; Celani, P.; Korona, T.; Rauhut, G.; Amos, R. D.; Bernhardsson, A.; Berning, A.; Cooper, D. L.; Deegan, M. J. O.; Dobbyn, A. J.; Eckert, F.; Hampel, C.; Hetzer, G.; Lloyd, A. W.; McNicholas, S. J.; Meyer, W.; Mura, M. E.; Nicklaß, A.; Palmieri, P.; Pitzer, R.; Schumann, U.; Stoll, H.; Stone A. J.; Tarroni, R.; T. Thorsteinsson.

[30] VaReCoF, Georgievskii, Y.; Klippenstein, S. J. Sandia National Laboratories and Argonne National Laboratory, 2006.

[31] Wardlaw, D. M.; Marcus, R. A. *Chem. Phys. Lett.* **1984**, *110*, 230, *J. Chem. Phys.* **1985**, *83*, 3462, *J. Phys. Chem.* **1986**, *90*, 5838.

[32] Georgievskii, Y.; Klippenstein, S. J. *J. Phys. Chem. A* **2003**, *107*, 9776.

[33] Jasper, A. W.; Klippenstein, S. J.; Harding, L. B., unpublished work.

[34] Curran, H.; Pitz, W. J., private communication.